Two-nucleon spectral function of 16O at high momenta.

Geurts, W.J.W.; Allaart, K.; Dickhoff, W.H.; Muther, H.

published in
Physical Review C
1996

DOI (link to publisher)
10.1103/PhysRevC.54.1144

document version
Publisher's PDF, also known as Version of record

Two-nucleon spectral function of ^{16}O at high momenta

W. J. W. Geurts and K. Allaart
Department of Physics and Astronomy, Vrije Universiteit, De Boelelaan 1081, 1081 HV Amsterdam, The Netherlands

W. H. Dickhoff
Department of Physics, Washington University, St. Louis, Missouri 63130

H. Müther
Institut für Theoretische Physik, Universität Tübingen, Auf der Morgenstelle 14, D-72076 Tübingen, Germany
(Received 13 March 1996)

A procedure for the calculation of the two-body spectral function of a finite nucleus is presented. This spectral function is used to calculate the longitudinal part of the ^{16}O$(e,e'pp)$ cross section assuming plane waves for the outgoing nucleons. Short-range correlation effects are included in the pair-removal amplitudes by adding corresponding defect wave functions that are obtained from the solution of the Bethe-Goldstone equation in the finite nucleus. The associated G matrix is used as the effective interaction in a large but finite model space to calculate the pair-removal amplitudes in a random-phase approach. The resulting spectral functions exhibit clear differences between different realistic interactions in the momentum range 2–5 fm^{-1} for the initial proton momenta. [S0556-2813(96)01309-X]

PACS number(s): 21.10.Jx, 21.30.Fe, 21.60.−n

I. INTRODUCTION

Detectable consequences of the presence of short-range correlations (SRC's) in low-energy nuclear phenomena have been notoriously hard to come by. Recent experimental work has probed the presence of high-momentum nucleons in the ground state by studying the removal of protons from shells near the Fermi energy by means of the $(e,e'p)$ reaction [1,2]. Earlier theoretical calculations performed in ^{16}O actually suggested that the consequences of SRC's, as reflected by the presence of high-momentum nucleons, can only be probed at high excitation energy in the hole nucleus ^{15}N [3,4]. Indeed, little evidence for the presence of high-momentum nucleons in both ^{207}Tl [1] and ^{15}N [2] at low excitation energy has been gathered. It remains to be verified experimentally whether an unambiguous signal of high-momentum protons in the nucleus can be isolated using the $(e,e'p)$ reaction.

Suggestions to explore SRC's in two-nucleon emission reactions go back to the work of Gottfried [5]. More recently, theoretical work has focused on the possibility of utilizing the $(e,e'2N)$ reaction to probe nucleon-nucleon correlations [6–8]. Practical descriptions of this reaction have been developed by the Pavia group [9–12]. Proceeding in a similar vein as in the analysis of the $(e,e'p)$ reaction, which yields information about the one-nucleon(-removal) spectral function, one may hope to learn about the two-nucleon (-removal) spectral function in two-nucleon-emission processes. The emission of two protons is particularly promising for studies of SRC's since the effect of meson-exchange currents and isobars is not expected to dominate the cross section under suitable kinematic conditions [10].

Experiments have been carried out for ^{12}C [13] and ^{16}O [14] to explore the feasibility of gaining insight into nucleon-nucleon correlations in finite nuclei using the $(e,e'pp)$ reaction. Triple-coincidence measurements involving protons with large initial momenta seem particularly suitable to provide information on SRC's. The scattered electron is then expected to transfer a virtual photon to one of these two protons which have large and opposite momenta and therefore a relatively small center-of-mass momentum. This strong correlation results from hard collisions due to the strong repulsive core of the nucleon-nucleon (NN) interaction. When one of the protons is removed by the absorption of the virtual photon, its partner will also leave the nucleus under the assumption that the energy transfer is mainly to the hit pair (the residual nucleus stays at a low excitation energy) [9]. It is therefore hoped that, if the coupling of the virtual photon to one nucleon is the dominant mechanism, the $(e,e'pp)$ process may be exploited as a useful tool to investigate these short-range correlation effects (see also Ref. [15]).

It is the purpose of the present paper to calculate the two-nucleon spectral function of ^{16}O for transitions to the low-lying states of the final ^{14}C nucleus, including the effects of short-range correlations. Modifications of the two-body spectral function, due to low-energy shell model correlations, will also be taken into account. In Sec. II of this paper the relevant theoretical ingredients are gathered which are needed to calculate the two-body spectral function. Section III contains a description of the two-step procedure which includes a folding of short-range correlation effects into a calculation of the two-body propagator in a configuration space large enough to deal adequately with long-range correlations. Details of the latter calculations are discussed in Sec. IV. Results for the two-nucleon spectral function and a first estimate of the corresponding longitudinal cross sections are presented in Sec. V, while some conclusions are drawn in Sec. VI.

II. SPECTRAL FUNCTIONS AND GREEN'S FUNCTIONS

An important ingredient in the description of the two-nucleon knockout reaction is the two-hole spectral function defined by

$$S^{hh}(\mathbf{p}_1,\mathbf{p}_2,\mathbf{p}_{1'},\mathbf{p}_{2'},\omega)=\sum_n \langle\Psi_0^A|a^\dagger_{\mathbf{p}_{1'}}a^\dagger_{\mathbf{p}_{2'}}|\Psi^{n,A-2}\rangle \times\langle\Psi^{n,A-2}|a_{\mathbf{p}_1}a_{\mathbf{p}_2}|\Psi_0^A\rangle \times\delta(\omega-(E^{0,A}-E^{n,A-2})), \quad (1)$$

where Ψ_0^A denotes the (0^+) ground state of the target system (^{16}O) and $\Psi^{n,A-2}$ denotes the nth excited state of the residual nucleus (^{14}C). In Eq. (1), $a^\dagger_{\mathbf{p}}$ ($a_{\mathbf{p}}$) represents the addition (removal) operator of a nucleon with momentum $\mathbf{p}$ (spin and isospin are implicit).

Since nuclear states have well-defined angular momentum and parity quantum numbers, it is useful to expand these operators into a basis with shell model quantum numbers according to

$$a_{\mathbf{p}}=\sum_\alpha \phi_\alpha(\mathbf{p})a_\alpha, \quad (2)$$

with $\alpha=\{n_\alpha,l_\alpha,j_\alpha,m_\alpha\}$. For the description of bound systems one can employ single-particle wave functions which correspond to Woods-Saxon or harmonic oscillator eigenstates. If the experimental energy resolution of the coincidence cross sections is sufficiently good, it is possible to identify contributions from individual low-lying final states, with well-defined angular momenta. It is therefore natural to introduce a pair wave function in angular momentum coupled form [16–18]

$$\Phi^{JM}_{cd}(\mathbf{p}_{1'},\mathbf{p}_{2'})=\sum_{m_\gamma m_\delta}(j_\gamma m_\gamma j_\delta m_\delta|JM)\phi_\gamma(\mathbf{p}_{1'})\phi_\delta(\mathbf{p}_{2'}), \quad (3)$$

where a Clebsch-Gordan coefficient is employed, and the indices c and d denote basis states without the magnetic quantum number: $a=\{n_a,l_a,j_a\}$. The spectral function (1) for final states with angular momentum J can now be written as

$$S^{hh}_J(\mathbf{p}_1,\mathbf{p}_2,\mathbf{p}_{1'},\mathbf{p}_{2'},\omega) =\sum_{abcd,M}\Phi^{*JM}_{cd}(\mathbf{p}_{1'},\mathbf{p}_{2'})S^-_{cdab;JM}(\omega)\Phi^{JM}_{ab}(\mathbf{p}_1,\mathbf{p}_2). \quad (4)$$

The two-nucleon-removal spectral function $S^-_{abcd;JM}$ may be calculated by constructing shell model wave functions for the initial and final nuclei and, subsequently, determining the matrix element of the angular-momentum-coupled two-nucleon-removal operator $(a_{\mathbf{p}_1}a_{\mathbf{p}_2})_{JM}$. A more direct method, which will be employed here, is to use the relation between the spectral function and the (imaginary part of the) two-particle Green's function:

$$S^-_{abcd;JM}(\omega)=\frac{-1}{\pi}\mathrm{Im}G^{II}_{abcd;JM}(\omega),\omega\leqslant E^{0,A-2}-E^{0,A}. \quad (5)$$

The latter describes the propagation of a pair of nucleons through the nuclear medium and contains information on both two-particle removal and two-particle addition. Its Lehmann representation, in angular-momentum-coupled form, is given by

$$\begin{aligned}G^{II}_{abcd;J}(\omega)&=\sum_n\frac{\langle\Psi_0^A||(a_{\tilde\beta}a_{\tilde\alpha})_J||\Psi_J^{n,A+2}\rangle\langle\Psi_J^{n,A+2}||(a^\dagger_\gamma a^\dagger_\delta)_J||\Psi_0^A\rangle}{\omega-(E_J^{n,A+2}-E^{0,A})+i\eta}\\&\quad-\sum_m\frac{\langle\Psi_0^A||(a^\dagger_\gamma a^\dagger_\delta)_J||\Psi_J^{m,A-2}\rangle\langle\Psi_J^{m,A-2}||(a_{\tilde\beta}a_{\tilde\alpha})_J||\Psi_0^A\rangle}{\omega-(E^{0,A}-E_J^{m,A-2})-i\eta}\\&=\sum_n\frac{Y^{n*}_{abJ}Y^n_{cdJ}}{\omega-(E_J^{n,A+2}-E^{0,A})+i\eta}\\&\quad-\sum_m\frac{X^{m*}_{cdJ}X^m_{abJ}}{\omega-(E^{0,A}-E_J^{m,A-2})-i\eta}.\end{aligned} \quad (6)$$

The symbols $\langle\cdots||\cdots||\cdots\rangle$ represent the reduced matrix elements [16–18] of the two-nucleon-removal and -addition tensor operators that are constructed by the angular momentum coupling of two one-nucleon-addition and -removal tensors [$a^\dagger_\alpha$ and $a_{\tilde\alpha}$, where $a_{\tilde\alpha}=(-)^{j_\alpha-m_\alpha}a_{-\alpha}$ and $-\alpha$ denotes $\{n_\alpha,l_\alpha,j_\alpha,-m_\alpha\}$, the time reverse of α]. The spectral function (1) may then be written as

$$\begin{aligned}S^{hh}_J(\mathbf{p}_1,\mathbf{p}_2,\mathbf{p}_{1'},\mathbf{p}_{2'},\omega)&=\sum_n\sum_{abcd,M}\Phi^{*JM}_{cd}(\mathbf{p}_{1'},\mathbf{p}_{2'})X^{n*}_{cdJ}X^n_{abJ}\Phi^{JM}_{ab}(\mathbf{p}_1,\mathbf{p}_2)\\&\quad\times\delta(\omega-(E^{0,A}-E_J^{n,A-2})).\end{aligned} \quad (7)$$

One reason to prefer a calculation of the amplitudes X via the Green's function (6) is that one may take advantage of experimental knowledge about the one-nucleon Green's functions:

$$\begin{aligned}g_{\alpha\beta}(\omega)&=\sum_n\frac{\langle\Psi_0^A|a_\alpha|\Psi_m^{A+1}\rangle\langle\Psi_n^{A+1}|a^\dagger_\beta|\Psi_0^A\rangle}{\omega-(E^{n,A+1}-E^{0,A})+i\eta}\\&\quad+\sum_m\frac{\langle\Psi_0^A|a^\dagger_\beta|\Psi_m^{A-1}\rangle\langle\Psi_m^{A-1}|a_\alpha|\Psi_0^A\rangle}{\omega-(E^{0,A}-E^{m,A-1})-i\eta}.\end{aligned} \quad (8)$$

These contain one-nucleon-removal amplitudes, which are probed in $(e,e'p)$ reactions [19–24]. These one-nucleon Green's functions form an important ingredient in the Bethe-Salpeter equation [18,25] for G^{II}:

$$G^{II}_{\alpha\beta\gamma\delta}(t_1,t_2,t_3,t_4)=i[g_{\alpha\gamma}(t_1-t_3)g_{\beta\delta}(t_2-t_4)-g_{\alpha\delta}(t_1-t_4)g_{\beta\gamma}(t_2-t_3)]$$
$$-\int_{-\infty}^{\infty}dt_1'dt_2'dt_3'dt_4'\sum_{\mu\nu\kappa\lambda}[g_{\alpha\mu}(t_1-t_1')g_{\beta\nu}(t_2-t_2')]\Gamma^{pp}_{\mu\nu\kappa\lambda}(t_1',t_2',t_3',t_4')G^{II}_{\kappa\lambda\gamma\delta}(t_3',t_4',t_3,t_4), \quad (9)$$

where Γ denotes the irreducible effective particle-particle interaction. From the one-nucleon-removal experiments one knows that the spectroscopic strength for the lowest states is typically only 50–70 % of the values predicted by the independent-particle shell model and that another 10–20 % is fragmented over the experimentally analyzed energy region of about 20 MeV. If one keeps only the first term on the right-hand side (RHS) of Eq. (9), a corresponding fragmentation is also predicted for the two-nucleon-removal strength and it is only the interaction term which may further influence G^{II}. The strong fragmentation of the one-nucleon removal strength is attributed to the strong coupling of single-particle motion to (low-energy) excitations of the residual nucleus [26–30].

In addition to this coupling at low energy, a 10–15% depletion of filled orbits is expected on the basis of nuclear-matter results for SRC's [31–37]. Recent calculations for ^{16}O [3,4,30] confirm this estimate. Related to this depletion is the appearance of high-momentum nucleons in the ground state. These high-momentum nucleons are expected to be observable at high missing energy in the $(e,e'p)$ reaction [3,4]. In the present work we focus on the high relative momenta of two-nucleon wave functions induced by SRC's. The preceding discussion suggests that, for a calculation of the high-momentum components of the two-nucleon spectral functions for discrete final states, both long- and short-range correlations should be taken into account. A method to deal with both aspects is presented and applied in the next sections.

III. INCLUSION OF SHORT- AND LONG-RANGE CORRELATIONS

A. Short-range correlations from the Bethe-Goldstone equation

In a pure mean-field approximation for ^{16}O, the expansion in Eq. (4) of the two-hole spectral function contains the contributions from the filled $1s$ and $1p$ shells only. The description of the high-momentum components due to SRC's requires the inclusion of a very large number of basis states, at least up to $100\hbar\omega$ in a harmonic oscillator basis [38]. The description of long-range correlations by solving a Bethe-Salpeter equation (9) within such a large space is not feasible, however. For this reason the complete basis is split into a model space $\mathcal{M}$, which is supposed to be large enough to accommodate long-range correlations, and a complementary space $\bar{\mathcal{M}}$, which is responsible for the high-momentum components due to SRC's. The justification for this procedure is that SRC's are caused by close encounters of two nucleons, which mainly depend on the nuclear density, and therefore are not very sensitive to details of the long-range structure. The latter, on the other hand, may be calculated within the space $\mathcal{M}$ with a suitable effective interaction in which the SRC's are incorporated at least in ladder approximation. This effective interaction can then be obtained by following Brueckner's individual pair approach [39,40] by solving the Bethe-Goldstone equation (BGE). Using the technique of Ref. [38] the equation for the correlated pair wave function,

$$|\Psi_{ab}\rangle=|\Phi_{ab}\rangle+\frac{\hat{Q}}{W-\hat{H}_0}\hat{V}|\Psi_{ab}\rangle, \quad (10)$$

is solved in the finite nucleus. In this equation the Pauli operator $\hat{Q}$ prohibits scattering into orbits of the finite shell model space $\mathcal{M}$, in which long-range correlations will be treated at a later stage. For instance, in the present calculation for ^{16}O, this space includes the $1s$ up to $2p1f$ harmonic oscillator shells. In Eq. (10), Φ_{ab} represents the uncorrelated shell model wave function, the indices a and b indicating quantum numbers of shell model orbits. The symbol W represents the propagation energy of the pair and $\hat{H}_0$ is the Hamiltonian without residual interaction. In this work, the energy W refers to the propagation of two holes which precludes the vanishing of the denominator in Eq. (10). Details of the solution of the BGE for a finite nucleus like ^{16}O have been given in Ref. [38].

From the solution of Eq. (10) one obtains the defect wave function as the difference between the correlated and uncorrelated pair wave function,

$$|\chi\rangle=|\Psi\rangle-|\Phi\rangle, \quad (11)$$

and the G matrix as the effective interaction in the space $\mathcal{M}$ according to

$$\langle\Phi^{JM}_{cd}|G|\Phi^{JM}_{ab}\rangle=\langle\Phi^{JM}_{cd}|V|\Psi^{JM}_{ab}\rangle. \quad (12)$$

The essential step taken in this work is to approximate the spectral function (7) by the expression

$$S^{hh}_J(\mathbf{p}_1,\mathbf{p}_2,\mathbf{p}_{1'},\mathbf{p}_{2'},\omega)$$
$$=\sum_{n,M}\sum_{ab,cd\in\mathcal{M}}\Psi^{*JM}_{cd}(\mathbf{p}_{1'},\mathbf{p}_{2'})X^{n*}_{cdJ}X^{n}_{abJ}$$
$$\times\Psi^{JM}_{ab}(\mathbf{p}_1,\mathbf{p}_2)\,\delta(\omega-E^{n,A-2}_J), \quad (13)$$

where the summation over orbits is limited to the finite shell model space $\mathcal{M}$ and the uncorrelated wave functions are replaced by the correlated ones [see Eq. (10)]. This is in line with the argument just given, that hard binary collisions, treated in the BGE and giving rise to high-momentum components, proceed independently of the long-range correlations. The latter are taken into account in the shell model amplitudes X within the limited space $\mathcal{M}$.

The defect function (11) is calculated for various partial waves of relative motion of the two nucleons. One must therefore expand the two-particle shell model wave functions in oscillator states of the relative and the center-of-mass momentum of the pair:

$$\mathbf{P}_{\rm c.m.}=\frac{\mathbf{p}_1+\mathbf{p}_2}{\sqrt{2}}, \quad \mathbf{p}_{\rm rel}=\frac{\mathbf{p}_1-\mathbf{p}_2}{\sqrt{2}}. \tag{14}$$

One obtains

$$\Phi^{JM}_{n_a l_a j_a n_b l_b j_b}(\mathbf{p}_1,\mathbf{p}_2) = \sum_{nlNLSJ'} C^{n_a l_a j_a n_b l_b j_b J}_{nlNLSJ'} \Phi^{J_f M_f}_{nlNLSJ'}(\mathbf{p}_{\rm rel},\mathbf{p}_{\rm c.m.}), \tag{15}$$

where the coefficients C in Eq. (15) are obtained by angular momentum recoupling and a Moshinsky transformation [17,41,42],

$$C^{n_a l_a j_a n_b l_b j_b J}_{nlNLSJ'} = \sum_{\lambda} (-)^{L+\lambda+J'+S} \hat{\lambda}\hat{J}'\hat{S}\hat{j}_a\hat{j}_b \begin{Bmatrix} l_a & l_b & \lambda \\ s_a & s_b & S \\ j_a & j_b & J \end{Bmatrix} \times \langle nlNL\lambda | n_a l_a n_b l_b \lambda\rangle \begin{Bmatrix} L & l & \lambda \\ S & J & J' \end{Bmatrix}, \tag{16}$$

with the notation $\hat{j}=\sqrt{2j+1}$. In this expression the nine-j symbol originates from the transformation of the coupling scheme

$$\mathbf{l}_a+\mathbf{s}_a=\mathbf{j}_a, \quad \mathbf{l}_b+\mathbf{s}_b=\mathbf{j}_b, \quad \mathbf{j}_a+\mathbf{j}_b=\mathbf{J} \tag{17}$$

to the alternative scheme

$$\mathbf{l}_a+\mathbf{l}_b=\lambda, \quad \mathbf{s}_a+\mathbf{s}_b=\mathbf{S}, \quad \lambda+\mathbf{S}=\mathbf{J}, \tag{18}$$

and the six-j symbol represents the recoupling from

$$\mathbf{l}+\mathbf{L}=\lambda, \quad \lambda+\mathbf{S}=\mathbf{J} \tag{19}$$

to

$$\mathbf{l}+\mathbf{S}=\mathbf{J}', \quad \mathbf{J}'+\mathbf{L}=\mathbf{J}. \tag{20}$$

The Talmi-Moshinsky transformation brackets, which presuppose that all states involved are of the harmonic oscillator form, may be found in the tables of Ref. [42]. An explicit expression for the more complicated case of unequal mass particles may be found in Ref. [43]. The partial-wave terms can be written in terms of the shell model wave functions according to

$$\Phi_{nN(lS)J'LJ_fM_f}(\mathbf{p}_{\rm rel},\mathbf{p}_{\rm c.m.}) = \sum_{\lambda} (-)^{L-\lambda+J'+S} \hat{\lambda}\hat{J}' \begin{Bmatrix} L & l & \lambda \\ S & J_f & J' \end{Bmatrix} \sum_{m,M_L,\mu,s_{a,z},s_{b,z},S_z} (lmLM_L|\lambda\mu)(s_a s_{a,z} s_b s_{b,z}|SS_z) \times (\lambda\mu SS_z|J_fM_f) R_{nl}(|\mathbf{p}_{\rm rel}|) Y_{lm}(\hat{\mathbf{p}}_{\rm rel}) R_{NL}(|\mathbf{p}_{\rm c.m.}|) Y_{LM_L}(\hat{\mathbf{p}}_{\rm c.m.}) \xi_{s_a s_{a,z}} \xi_{s_b s_{b,z}}, \tag{21}$$

where R_{nl} represents radial wave functions and Y_{lm} the spherical harmonics. The symbols ξ denote the spin wave functions. In the present application wave functions are always calculated in complex conjugated pairs; cf. Eq. (7). This means that in the spectral function the spin part can be dealt with explicitly, using $\xi^*_{ss_z}\xi_{ss_z'}=\delta_{s_z s_z'}$. So the factor $(s_a s_{a,z} s_b s_{b,z}|SS_z)$ will drop out together with the summation over $s_{a,z}$ and $s_{b,z}$ due to the condition that the total spin S be the same in both two-body wave functions for each term of the spectral function (7).

The SRC's are now introduced by the addition of the defect wave functions from the BGE to the uncorrelated partial waves (for the relative motion):

$$R^{SJ'}_{nl}(\mathbf{p}_{\rm rel}) = \phi^{SJ'}_{nl}(\mathbf{p}_{\rm rel}) + \sum_{l'} \chi^{SJ'}_{nl,l'}(\mathbf{p}_{\rm rel}), \tag{22}$$

with $l'=l,l\pm2$. The contribution $l'=l\pm2$ arises for triplet $(S=1)$ states, due to tensor components in the NN interaction. Defect wave functions obtained for the Bonn-A, Bonn-C [44], and Reid-soft-core [45] NN potentials are displayed in Fig. 1.

B. Alternative: SRC's represented by correlation functions

An alternative method to introduce short-range correlations in the two-particle-removal amplitudes is inspired by the correlated basis function (CBF) method [46]. At the variational level the correlated many-body wave function is related to the uncorrelated (A-body) wave function by [47–49]

$$\Psi^A(\mathbf{r}_1,\ldots,\mathbf{r}_A) = \sum_k \prod_{i<j} f_k(|\mathbf{r}_i-\mathbf{r}_j|) O_k \Phi^A(\mathbf{r}_1,\ldots,\mathbf{r}_A), \tag{23}$$

where the correlation functions and corresponding operators are denoted by f_k and O_k, respectively. Only two-body correlations are explicitly considered in Eq. (23). The Pavia group has proposed [9] to use these correlation functions to modify the short-range behavior of the relative wave function of the removed pair

$$\Psi(\mathbf{r}_1,\mathbf{r}_2) = \sum_k f_k(|\mathbf{r}_1-\mathbf{r}_2|) O_k \Phi(\mathbf{r}_1,\mathbf{r}_2). \tag{24}$$

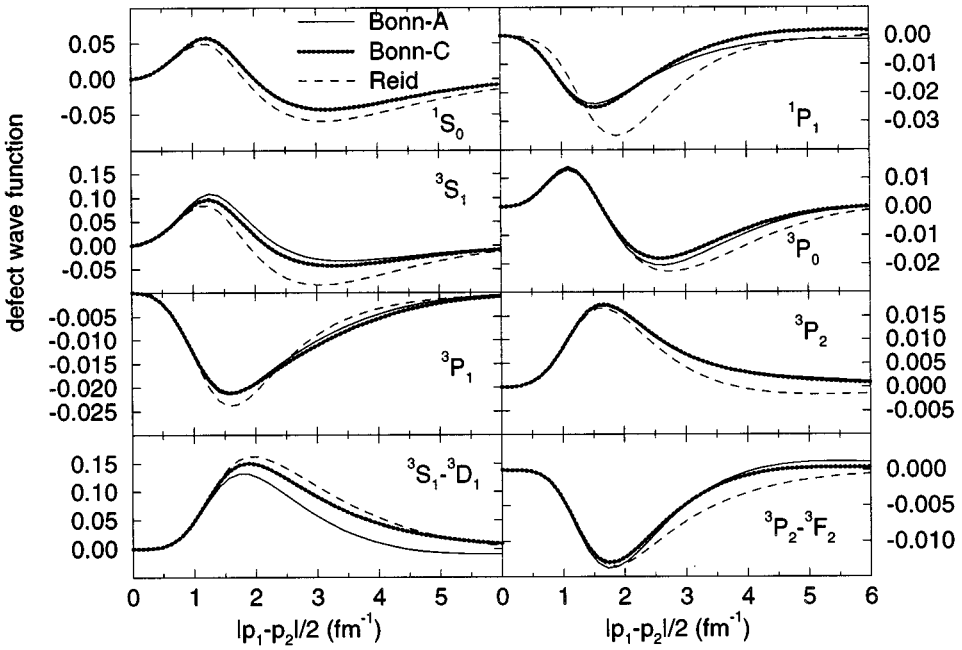

FIG. 1. Defect functions [see Eq. (11)] calculated for different partial waves by solving the Bethe-Goldstone equation (10) for ^{16}O, by the method of Ref. [38]. The lowest two panels contain the tensor defect functions $^3S_1-{}^3D_1$ (left) which contribute to the $^3S_1$ partial wave and $^3P_2-{}^3F_2$ which contribute to the $^3P_2$ partial wave. Results are plotted for the Bonn-A, Bonn-C, and Reid-soft-core potential.

When only central correlations are considered in Eqs. (23) and (24) one refers to Jastrow wave functions [47]. Jastrow correlation functions, calculated by Clark [50] for the Kallio-Kolltveit (KK) [51] and Ohmura-Morita-Yamada (OMY) [52] interactions, have been used by the Pavia group to calculate $(e,e'2N)$ cross sections [9–12]. In general, all the operators that are important in the nuclear two-body interaction should be included in Eq. (24) [49,53]. The eight most relevant operators are listed in Table I. Recent variational Monte Carlo calculations for ^{16}O [54] have generated a set of correlation functions appropriate for these operators. It is important to keep in mind that the use of correlation functions is plausible but does not represent a consistent CBF treatment of the two-nucleon-removal amplitudes. Such a consistent CBF treatment has been developed for the one-nucleon spectral function for nuclear matter [32,36].

A recent application of Green's function techniques to the calculation of relative two-nucleon wave functions in nuclear matter also allows the extraction of a correlation function [55,56]. Since SRC's are expected to depend mainly on the local density, it is meaningful to consider the application of this correlation function and compare its result with those obtained with the defect functions from a Bethe-Goldstone equation. The work in Refs. [55,56] also demonstrates that the spectral function in coordinate space can be interpreted as the product of the in-medium wave functions of the removed pair at a given energy. This suggests that the use of correlation functions might be fruitfully compared to results obtained by using defect wave functions.

TABLE I. List of operators which dominate the nuclear interaction. Corresponding correlation functions are determined in Ref. [54] by a variational Monte Carlo calculation for ^{16}O. The tensor operator S_{12} is defined as $3(\boldsymbol{\sigma}_1\cdot\hat{\mathbf{r}}_{12})(\boldsymbol{\sigma}_2\cdot\hat{\mathbf{r}}_{12})-\boldsymbol{\sigma}_1\cdot\boldsymbol{\sigma}_2$.

1	$\boldsymbol{\sigma}_1\cdot\boldsymbol{\sigma}_2$	S_{12}	$\mathbf{l}\cdot\mathbf{S}$
$\boldsymbol{\tau}_1\cdot\boldsymbol{\tau}_2$	$\boldsymbol{\sigma}_1\cdot\boldsymbol{\sigma}_2(\boldsymbol{\tau}_1\cdot\boldsymbol{\tau}_2)$	$S_{12}(\boldsymbol{\tau}_1\cdot\boldsymbol{\tau}_2)$	$\mathbf{l}\cdot\mathbf{S}(\boldsymbol{\tau}_1\cdot\boldsymbol{\tau}_2)$

Such a connection between defect functions and correlation functions may be made by the observation that the correlated wave function calculated with the defect function (11) can also be expressed in terms of the correlation functions in Eq. (24):

$$\Psi(r)=\Phi(r)+\chi(r)=\mathcal{O}(r)\Phi(r). \tag{25}$$

For the $T=1$ case, appropriate for two protons, the correlation operator is given by

$$\mathcal{O}(r_{12})=f_c(r_{12})+f_\sigma(r_{12})\boldsymbol{\sigma}_1\cdot\boldsymbol{\sigma}_2+f_{ls}(r_{12})\mathbf{l}\cdot\mathbf{S}+f_t(r_{12})\hat{S}_{12}, \tag{26}$$

where the tensor operator $\hat{S}_{12}$ is given by the expression $3(\boldsymbol{\sigma}_1\cdot\hat{\mathbf{r}}_{12})\ (\boldsymbol{\sigma}_2\cdot\hat{\mathbf{r}}_{12})\ -\ \boldsymbol{\sigma}_1\cdot\boldsymbol{\sigma}_2$. In order to disentangle the different contributions to the correlated wave function, the following matrix elements are needed for proton-proton $(T=1)$ wave functions:

$$\langle\Phi_{l'}^{S'J}|\mathbf{1}|\Phi_l^{SJ}\rangle=\delta_{ll'}\delta_{SS'},$$

$$\langle\Phi_{l'}^{S'J}|\boldsymbol{\sigma}_1\cdot\boldsymbol{\sigma}_2|\Phi_l^{SJ}\rangle=\delta_{ll'}\delta_{SS'}(2S(S+1)-3),$$

$$\langle\Phi_{l'}^{S'J}|\mathbf{l}\cdot\mathbf{S}|\Phi_l^{SJ}\rangle=\delta_{ll'}\delta_{SS'}\frac{1}{2}(J(J+1)-l(l+1)-S(S+1)),$$

$$\langle \Phi_{l'}^{S'J}|\hat{S}_{12}|\Phi_{l}^{SJ}\rangle = \delta_{S1}\delta_{S'1} 2\sqrt{30}(-)^{J+1}\sqrt{2l+1}\sqrt{2l'+1} \times \begin{Bmatrix} J & 1 & l' \\ 2 & l & 1 \end{Bmatrix} \begin{pmatrix} l' & l & 2 \\ 0 & 0 & 0 \end{pmatrix}.$$

These results can be applied to find the correlated wave function for different quantum numbers l, S, and J. Using the partial-wave notation $^{2S+1}l_J$ for $l=S,P,D,F$, the correlated waves can then be written as

$$\Psi(^1S_0) = (f_c - 3f_\sigma)\Phi(^1S_0), \tag{27}$$

$$\Psi(^3P_0) = (f_c + f_\sigma - 2f_{lS} - 4f_t)\Phi(^3P_0), \tag{28}$$

$$\Psi(^3P_1) = (f_c + f_\sigma - f_{lS} + 2f_t)\Phi(^3P_1), \tag{29}$$

$$\Psi(^3P_2) = \left(f_c + f_\sigma + f_{lS} - \frac{2}{5}f_t\right)\Phi(^3P_2) + 6\sqrt{6}f_t\Phi(^3F_2), \tag{30}$$

$$\Psi(^1D_2) = (f_c - 3f_\sigma)\Phi(^1D_2), \tag{31}$$

$$\Psi(^3F_2) = \left(f_c + f_\sigma - 8f_{lS} - \frac{8}{5}f_t\right)\Phi(^3F_2) + 6\sqrt{6}f_t\Phi(^3P_2). \tag{32}$$

The correlation functions can be extracted, if the defect functions are transformed to coordinate space, by means of a Fourier-Bessel transformation. For instance, Eq. (27) then yields

$$\tilde{f}_c(r) - 3f_\sigma(r) = \frac{\chi_{^1S_0}(r)}{R_{00}(r)}, \tag{33}$$

where $\tilde{f}_c$ is defined as $f_c - 1$. Since the sum of Eq. (28), 3 times Eq. (29) and 5 times Eq. (30), is independent of f_{lS} and f_t, this linear combination together with Eq. (33) is used to extract the central and spin correlation function f_c and f_σ. By elimination of these from the set (28)–(30) also the spin-orbit and the tensor correlation functions f_{lS} and f_t can be obtained. These functions are plotted in Fig. 2 for the Reid potential.

Before we discuss these results more in detail we should mention that certain approximations have to be made to arrive at this representation of the defect function in terms of local correlation functions. As a result of the Pauli operator $\hat{Q}$ occurring in Eq. (10), the defect function calculated for a finite nucleus does not simply factorize into a product of wave functions depending on relative and on center-of-mass coordinates. In order to arrive at a defect function just depending on a relative coordinate, we had to average over the center-of-mass variable. Furthermore, it should be noticed that for the determination of the various correlation functions we have to consider also partial waves with orbital angular momentum $l \geq 1$. Since the effects of correlations are much less significant in these partial waves than for the $l=0$ partial waves, the resulting correlation function could be affected by inaccuracies in these channels.

Nevertheless, the comparison of these correlation functions deduced from the defect wave functions for finite nuclei with those obtained in nuclear matter [55,56] for the same Reid potential (dashed line in Fig. 3) is quite reasonable. Note that the correlation function for the $^1S_0$ partial

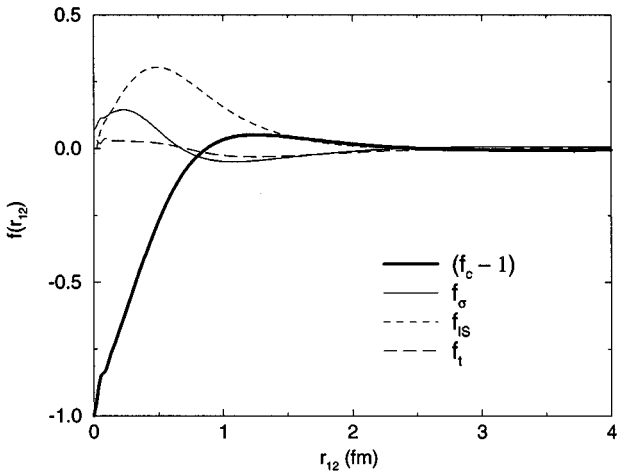

FIG. 2. Correlation functions in coordinate space that are related to the defect functions of Fig. 1 for the Reid-soft-core potential. This relation results in the same correlated wave function [cf. Eq. (25)] and involves the solution of Eqs. (27)–(30) together with Eq. (33).

wave, shown in Fig. 3, is related to the components displayed in Fig. 2 by the relation (27). In Fig. 3 also the correlation functions for the older KK [51] and OMY [52] potentials calculated by Clark [50] are displayed. Especially the correlation function calculated for the OMY potential gives a more pronounced suppression of the relative wave function at short distances than is the case for the Reid potential.

If one assumes, as is done in variational calculations, that correlation effects can be described in terms of correlation functions f_k, depending on the relative distance, which are the same in the different partial waves, then the formulas (31) and (32) can be used to construct the $^1D_2$ and $^3F_2$ defect functions. We find that the $^1D_2$ and $^3F_2$ defect functions of Fig. 1 are smaller than the ones constructed with Eqs. (31) and (32). The latter $^1D_2$ defect function is about a factor of 2 too large, while the $^3F_2$ differs orders of magnitude, but its construction from Eq. (32) is numerically inaccurate due to the small size of the defect function. It seems,

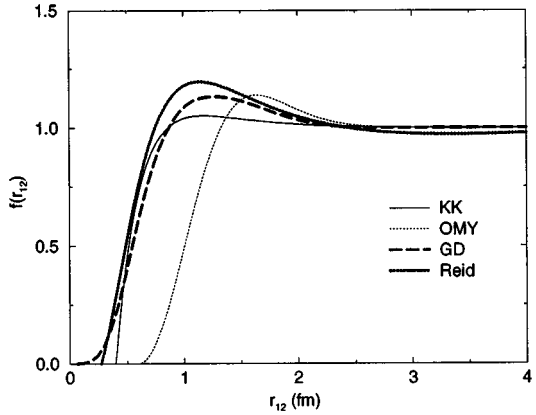

FIG. 3. Correlation functions obtained by a variational calculation [50] for the Kallio-Kolltveit (KK) [51] (solid line) and Ohmura-Morita-Yamada (OMY) [52] (dotted line) potentials. The thick dashed line corresponds to the correlation function calculated in Refs. [55,56] for the $^1S_0$ partial wave in nuclear matter with the Reid [45] potential.

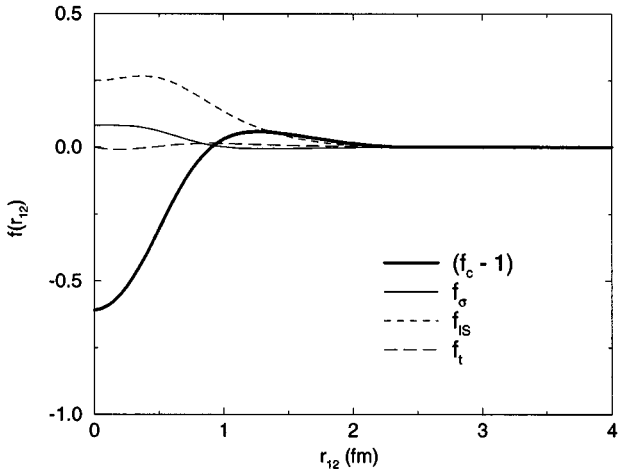

FIG. 4. Correlation functions for the Argonne v_{14} potential [57] as obtained in Ref. [54]. Note that the definition of our correlation operator (26) differs from the one used in Ref. [54].

therefore, that correlation functions, chosen to reproduce the correlations in the S wave correctly, exaggerate correlation effects in higher l components.

The elaborate variational Monte Carlo calculations of Ref. [54] yield correlation functions for central, spin, spin-orbit, and tensor correlations. Results obtained for the Argonne v_{14} potential [57] are displayed in Fig. 4. The effect of SRC's in these functions can be investigated in the present approach if the correlation functions are transformed to the form of defect functions. This transformation implies a Fourier-Bessel transform and the algebraic manipulations described by Eqs. (27)–(30). The results of this transformation are shown in Fig. 5. There is a reasonable agreement between the Reid and Argonne v_{14} potentials for high relative momenta, but for low momenta they differ. As discussed before, defect functions calculated within the finite nucleus do not simply factorize into a relative and a center-of-mass part. Since this problem originates from the Pauli operator, it is particularly severe for low momenta already present in the uncorrelated wave functions. This might be the explanation for the discrepancy at low momenta. In addition, one should keep in mind that the Argonne potential [57] does not go to infinity at zero relative distance but has a finite core. This results in a central correlation function which does not become equal to -1 for zero relative distance (see Fig. 4) as is the case for the Reid potential (see Fig. 3).

IV. LONG-RANGE CORRELATIONS IN THE DRESSED RPA

The shell model two-particle-removal amplitudes X_{ab}^{nJ} are obtained within the adopted model space $\mathcal{M}$ by solving the Bethe-Salpeter equation (9) for the two-nucleon propagator in dressed random phase approximation (DRPA) [28]. This implies that the dressed one-body propagators g that occur in Eq. (9) are calculated first by solving the Dyson equation [30]

$$g_{\alpha\beta}(\omega)=g^0_{\alpha\beta}(\omega)+\sum_{\gamma\delta} g^0_{\alpha\gamma}(\omega)\Sigma^*_{\gamma\delta}(\omega)g_{\delta\beta}(\omega). \quad (34)$$

As discussed in Ref. [30], the irreducible self-energy Σ^* includes a Hartree-Fock term containing the G matrix as an energy-dependent interaction plus a term of second and higher order in this interaction, which accounts for the coupling of the hole propagator to two-particle–one-hole and two-hole–one-particle propagation. The Dyson equation and the corresponding self-energy are given in Fig. 6. The results for the calculated propagator may be compared with the measured spectral function in the $(e,e'p)$ experiment on ^{16}O [24]. We have found [30] that within a model space of four major shells employing a G-matrix interaction con-

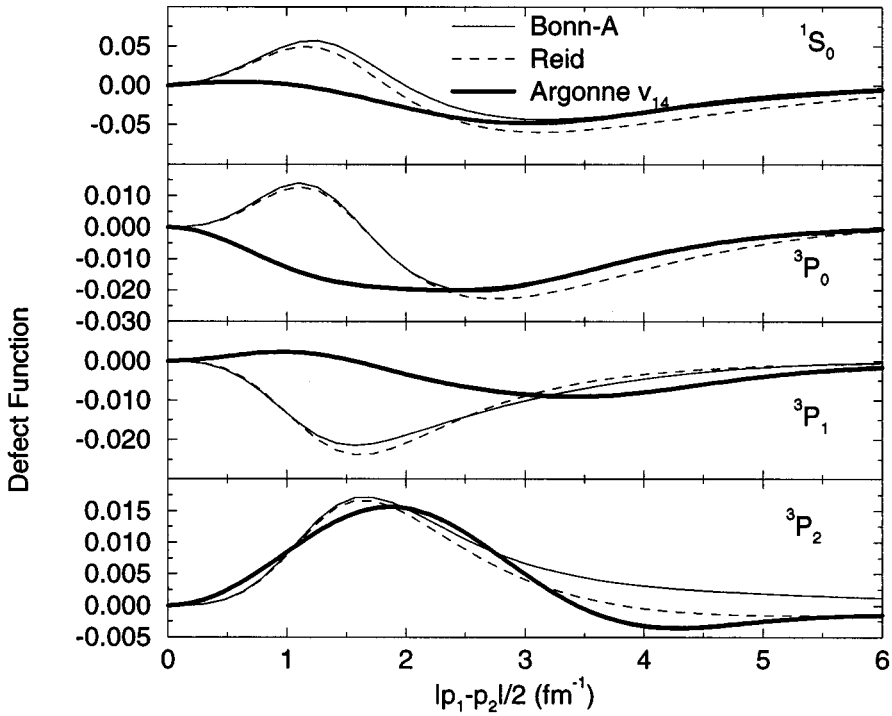

FIG. 5. Defect functions corresponding to the correlation functions of Fig. 4 for the Argonne v_{14} potential are compared with defect functions obtained from the Bethe-Goldstone equation using the Bonn-A and Reid-soft-core potentials (see also Fig. 1).

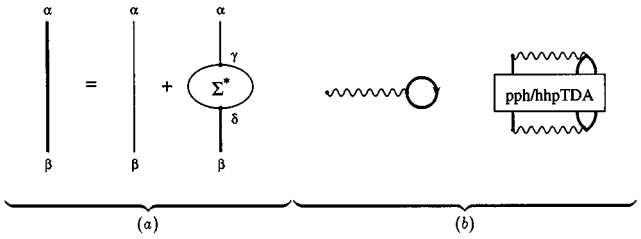

FIG. 6. Part (a) depicts the Dyson equation for the dressed one-body propagator. Part (b) shows the corresponding irreducible self-energy Σ^* which is approximated by the Hartree-Fock term with G-matrix interaction plus higher-order terms, including all interactions between two holes and one particle or two particles and one hole in the Tamm-Dancoff approximation [30,65].

structed from the Bonn-C potential, the distributions of knockout strength from the p shells, as a function of the energy of the final state in ^{15}N, are rather well reproduced. However, the largest spectroscopic factors for the low-energy states are not yet sufficiently reduced relative to the independent-particle shell model values. We obtain the reduction factors 0.77 for the $\frac{1}{2}^-$ and 0.76 for the $\frac{3}{2}^-$ states, while the analysis of the experimental data [24] yields 0.65 ± 0.05 and 0.63 ± 0.05, respectively. As a result, the first term in Eq. (9) and the corresponding contribution to the two-body spectral function (4) will be overestimated at low energy. For example, a 2^+ configuration built with a $p\frac{1}{2}$ and $p\frac{3}{2}$ hole contains just the product of the above spectroscopic factors. This product will be too large when our calculated one-body Green's functions g are inserted into the Bethe-Salpeter equation (9) for G^{II}. This could be improved by reducing the residues of the dominant pole terms in Eq. (8) to match the $(e,e'p)$ spectroscopic factors. We have not done this in the following, since our main aim is to investigate the gross features of the two-nucleon-removal strength and compare the high-momentum components obtained with different NN interactions.

The BSE (9) for G^{II} is solved in the space $\mathcal{M}$ with the G matrix as the effective interaction Γ. The difference with the conventional RPA is reflected in the use of dressed single-particle propagators g. The method to solve the equations has been discussed in Ref. [58]. The amplitudes for each discrete final state are extracted from the full two-proton propagator with the use of a contour integration in the complex energy plane as discussed in Ref. [59].

V. TWO-HOLE SPECTRAL FUNCTION OF ^{16}O AND THE LONGITUDINAL $(e,e'pp)$ CROSS SECTION

A. Final states in ^{14}C

Triple-coincidence measurements of the scattered electron and the two knocked-out protons with sufficient energy resolution may determine the cross sections for low-lying, discrete final states in ^{14}C separately. It is therefore useful to consider results for the individual low-lying transitions to ^{14}C. Results for the low-energy spectrum of ^{14}C, obtained from the DRPA equation with a G-matrix interaction deduced from the Bonn-C potential, are listed in Table II, together with the amplitudes X^J_{ad} of the dominant configurations. The squares of these amplitudes do not add up to 1, but rather to a number comparable with the product of two spectroscopic factors as discussed in the previous section.

TABLE II. Calculated energies and two-proton-removal amplitudes from ^{16}O for states of ^{14}C that are expected to be strongly populated in the ^{16}O$(e,e'pp)$ reaction. The calculation is performed by solving the Bethe-Salpeter equation for the two-particle Green's function (9) in the dressed random phase approximation (DRPA) [28] within a model space of the $1s$ up to the $2p1f$ shells. The G matrix derived from the Bonn-C potential is used as the effective interaction. The experimental energies are taken from Ref. [60] .

J^π	$E^*_{\rm calc}$ (MeV)	Main amplitudes (X_{ab})	$E^*_{\rm expt}$ (MeV)
0^+	0	$0.77*(p\frac{1}{2})^{-2}, 0.18*(p\frac{3}{2})^{-2}$	0
2^+	5.87	$-0.77*(p\frac{1}{2}p\frac{3}{2})^{-1}, 0.11*(p\frac{3}{2})^{-2}$	7.01/8.32
1^+	7.19	$0.76*(p\frac{1}{2}p\frac{3}{2})^{-1}$	11.31
0^+	12.00	$0.15*(p\frac{1}{2})^{-2}, -0.76*(p\frac{3}{2})^{-2}$	9.75
2^+	13.14	$0.10*(p\frac{1}{2}p\frac{3}{2})^{-1}, 0.76*(p\frac{3}{2})^{-2}$	

A comparison with the experimental ^{14}C spectrum [60] reveals in addition to states with energies and angular-momentum–parity quantum numbers (J^π), which can be interpretated as two-proton holes, e.g., in the $1p$ shells, also states that must be ascribed to more complicated mechanisms. For instance, the 1^- state at 6.094, 0^+ at 6.589, and 3^- at 6.728 MeV are clearly reminiscent of similar states in ^{16}O at 7.117, 6.049, and 6.130 MeV [61], respectively. It is therefore natural to interpret these states as excitations in ^{14}C of the ^{16}O core. These states, which do not allow a simple two-hole interpretation, are expected to be hardly populated in two-proton knockout from ^{16}O. This expectation is confirmed by a two-proton pickup experiment ^{16}O$(n,^3$He) in which only the ^{14}C ground state and 2^+ state at about 7 MeV were clearly visible [60,61].

Much clearer, though indirect, information is available from the isospin mirror reaction $^{16}O(p,t)^{14}$O [62,63]. In these experiments the strongly populated states of ^{14}O are the 0^+ ground state and the 2^+ states at 6.59 MeV and 7.78 MeV, respectively. No 1^+ state, composed of a $p\frac{1}{2}$ and a $p\frac{3}{2}$ hole, is seen in these reactions because in this configuration the relative wave function must correspond to $^3P_1$, whereas in the picked-up triton one has predominantly a $^1S_0$ configuration. As a result, there is no experimental information about this state, but we consider the 1^+ state at 11.31 MeV in ^{14}C as a likely candidate for a 1^+ two-proton–hole $(1p\frac{1}{2};1p\frac{3}{2})^{-1}$ configuration. Other two-proton–hole states in ^{14}C are expected at higher excitation energies. The strength of the negative parity configurations is spread over a larger energy region; cf. also Fig. 7.

Since we are interested in the high-momentum components of the two-proton spectral function, in order to obtain information on the SRC's, one must address the question, which final states are most strongly populated by the removal of a correlated $^1S_0$ proton pair from the ^{16}O ground state? For large relative momenta the $^1S_0$ partial wave has a much larger defect function than the ^3P or higher partial waves; cf. Fig. 1. Therefore it is to be expected that the strength distribution for the knockout of a strongly correlated proton-proton pair, as a function of energy, follows the pattern of the $^1S_0$-removal spectral function

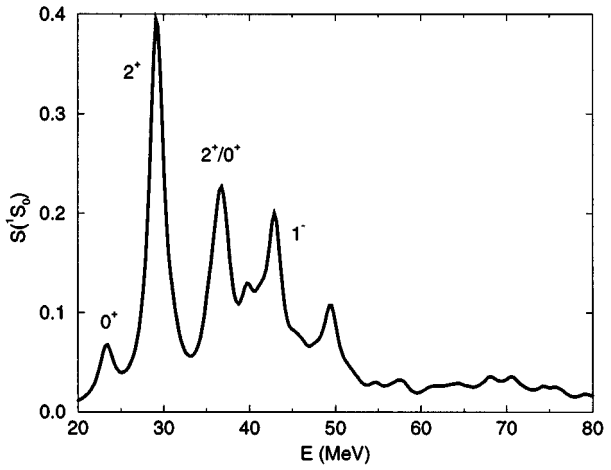

FIG. 7. Calculated spectral function (35) for the removal of a $^1S_0$ pair from the nucleus ^{16}O as a function of the energy E of the final state in ^{14}C relative to the ground state energy of ^{16}O (the first 0^+ corresponds to the two-proton separation energy). The plot represents the removal probability for a $^1S_0$ pair with radial quantum numbers $n=0$ for the relative motion and orbital angular momentum of the center of mass L equal to the total angular momentum of the final state in ^{14}C. The peak labeled with ''$2^+/0^+$,'' on the slope of the beginning 1^- distribution, has a 0^+ part slightly smaller than the ground state and a 2^+ part almost one third of the first 2^+.

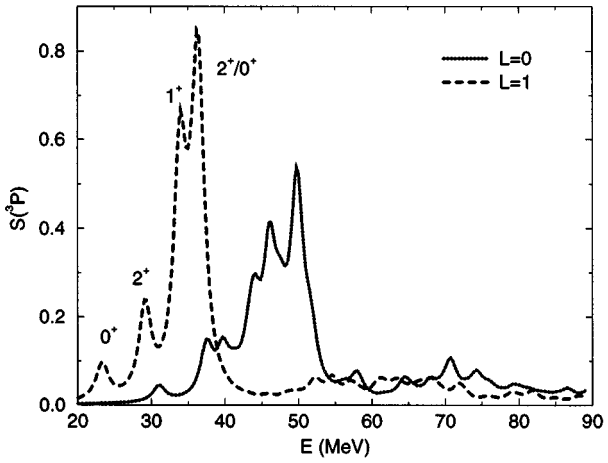

FIG. 8. Spectral function for the removal of a ^3P pair from ^{16}O. Additional quantum numbers of the pair correspond to $n=0$, $N=0$. Contributions for the center-of-mass orbital angular momentum L are indicated separately. The $L=0$ contribution (solid line) consists solely of negative parity states, while the $L=1$ contribution (dashed line) consists exclusively of positive parity states.

$$S_{^1S_0}(\omega)=\sum_m |\langle {}^{14}\mathrm{C}^m|(aa)_{^1S_0}|{}^{16}\mathrm{O}\rangle|^2\delta(\omega-E^m), \quad (35)$$

in which the operator $(aa)_{^1S_0}$ annihilates two particles coupled to $^1S_0$. This removed pair is further characterized by the radial quantum numbers n of the relative motion and the quantum numbers N and L of its center-of-mass motion. The spectral function (35) can be expressed in terms of the recoupling coefficients of Eq. (16) and the two-nucleon-removal amplitudes X given in Eq. (6) by a straightforward recoupling [16]:

$$S_{^1S_0}(\omega)=\sum_{m,J}\sum_{ab,cd} X^m_{ab}\sum_{ij}\widetilde{C}^{ab;J}_{Si}\widetilde{C}^{cd;J}_{Sj}X^m_{cd}\delta(E-E^m_J), \quad (36)$$

where the coupling coefficients $\widetilde{C}$ are defined (for general partial waves) as

$$\widetilde{C}^{ab;J}_{SnlNL\lambda}=\sum_{J'}(-)^{L-\lambda+J'+S}\begin{Bmatrix} L & l & \lambda \\ S & J & J' \end{Bmatrix} C^{ab;J}_{nNL(lS)J'}. \quad (37)$$

In Eq. (36) the spin S is set to zero. The easiest way to calculate the $^1S_0$-hole spectral function (35) is to rewrite the expression (35) in the form

$$S_{^1S_0}(\omega)=\frac{1}{\pi}\mathrm{Im}\sum_J (2J+1)v_{ab;J}G^{II}_{ab;cdJ}(\omega)v_{cd;J}, \quad (38)$$

where the vector $v_{ab;J}$ is obtained by inverting Eq. (37) with fixed values of n, N, and L for a given $(lS)J'$. In the calculations presented here, n, N, and L are chosen to have the lowest possible values. The advantage of rewriting Eq. (36) in the form of Eq. (38) lies in its similarity to the expression for the particle-hole response functions [28]. The spectral function (38) can now be calculated, using a continuous RPA method (calculate G^{II} with $\omega\rightarrow\omega+i\Delta$, where Δ is a finite energy), which avoids the intermediate step of calculating the amplitudes X.

The resulting $^1S_0$-pair-removal spectral function (35) is plotted in Fig. 7. The strongest peak at low excitation energy comes from the 2^+_1 state; cf. Table II. It is much stronger than that for the 0^+ ground state, partly due to the factor $2J+1$. The smaller peak around 12 MeV excitation energy, on the slope of the beginning 1^- distribution, has a 0^+ part slightly smaller than the ground state and a 2^+ part almost one-third of the first 2^+. Experimentally [61,60] the 2^+_2 state is at 8.32 MeV and the 0^+_2 state at 9.75 MeV, and so they could be separated with sufficiently good energy resolution. The 1^- contribution is spread over a wide energy region. Analogous to expression (35), a ^3P-pair-removal spectral function may be defined (putting $l=1$ and $S=1$). This function is plotted in Fig. 8. In this case the contributions with different center-of-mass angular momenta L show up mainly at different energies.

B. Spectral function for the lowest 0^+ and 2^+ states

One of the goals of the present study is to provide a sensible estimate of the $(e,e'pp)$ cross section. In the next subsection we will discuss the calculation of the longitudinal part of this cross section. In the analysis of the $(e,e'pp)$ data on ^{12}C at NIKHEF-K [64,9], the virtual photon is assumed to couple to one of the detected protons. This approximation can be understood by considering the transition matrix element of the nuclear charge operator in momentum space,

$$\hat{\rho}(\mathbf{q}) = e \sum_{\mathbf{p}'} a^{\dagger}_{\mathbf{p}'+\mathbf{q}} a_{\mathbf{p}'} \tag{39}$$

(with spin implicit in the summation), between the initial state Ψ_0^A and an approximate final state of the form

$$|\Psi_{\text{final}}\rangle = a^{\dagger}_{\mathbf{p}_1'} a^{\dagger}_{\mathbf{p}_2'} |\Psi^{n,A-2}\rangle. \tag{40}$$

This final state contains two plane-wave protons and an exact state $\Psi^{n,A-2}$ for the system with two protons removed. In calculating the matrix elements of the transition charge operator one obtains

$$\begin{aligned}\langle \Psi_{\text{final}}|\hat{\rho}(\mathbf{q})|\Psi_0^A\rangle &= \langle \Psi^{n,A-2}|a_{\mathbf{p}_2'} a_{\mathbf{p}_1'-\mathbf{q}}|\Psi_0^A\rangle + \langle \Psi^{n,A-2}|a_{\mathbf{p}_2'-\mathbf{q}} a_{\mathbf{p}_1'}|\Psi_0^A\rangle,\end{aligned} \tag{41}$$

assuming that one of the detected protons absorbs the momentum **q**. To obtain the contribution to the cross section one requires the square of this matrix element. This yields four terms, each representing a particular term of Eq. (1). It is therefore clear that the appropriate expression to consider is the quantity

$$\begin{aligned}\hat{S}(\mathbf{p}_1',\mathbf{p}_2',E) = {} & S(\mathbf{p}_1'-\mathbf{q},\mathbf{p}_2',\mathbf{p}_1'-\mathbf{q},\mathbf{p}_2',E) \\ & + S(\mathbf{p}_1'-\mathbf{q},\mathbf{p}_2',\mathbf{p}_1',\mathbf{p}_2'-\mathbf{q},E) \\ & + S(\mathbf{p}_1',\mathbf{p}_2'-\mathbf{q},\mathbf{p}_1'-\mathbf{q},\mathbf{p}_2',E) \\ & + S(\mathbf{p}_1',\mathbf{p}_2'-\mathbf{q},\mathbf{p}_1',\mathbf{p}_2'-\mathbf{q},E),\end{aligned} \tag{42}$$

where the vector **q** is the momentum of the virtual photon. A sensible way to plot $\hat{S}$ is to fix the angles of the momenta at some reasonable configuration of detectors, e.g., corresponding to the measurements at NIKHEF [14]. As an example, we have plotted in Fig. 9 the corresponding two-proton spectral function [without the delta function in Eq. (1)] at the energy of the first 0^+ and 2^+ states, for the high-momentum parts of Eq. (42) obtained with the Reid-soft-core and Bonn-A potentials. In the plots labeled ''No SRC'' harmonic oscillator states have been used for the relative wave functions in the spectral function. As expected, one observes that these give no contribution at higher momenta. The high-momentum part of the spectral function is about a factor of 2 larger for the Reid-soft-core potential than for the Bonn-A potential in the momentum range around 3–5 fm^{-1}. The short-range correlations give rise to a spectral function which is clearly distinct from the one without SRC's. In Fig. 10 the spectral strength for the same states is shown using Bonn-C defect functions. No significant difference with the Bonn-A calculation is observed. Corresponding results for the KK and OMY correlation functions, also shown in Fig. 10, yield a significantly larger spectral strength for the transition to the ground state, apparent already at lower momenta. The OMY results for the transition to the first 2^+ state also exhibit stronger SRC effects than the ones obtained with more realistic potentials.

C. Longitudinal $(e,e'pp)$ cross section in a plane-wave approximation

In the spectator model with a plane-wave approximation for the outgoing protons [9] (see previous discussion), the longitudinal contribution to the eightfold differential cross section is proportional to the zero-zero part of the hadronic tensor and given by

$$\begin{aligned}&\frac{d^8\sigma}{dp_0' d\Omega_0' dE_1' d\Omega_1' d\Omega_2'} \\ &\quad = K 2\varepsilon_L [G_E^p(q_\mu^2)]^2 |\langle \Psi_n^{A-2}|a_{\mathbf{p}_1'-\mathbf{q}} a_{\mathbf{p}'_2}|\Psi_0^A\rangle \\ &\qquad + \langle \Psi_n^{A-2}|a_{\mathbf{p}_1'} a_{\mathbf{p}'_2-\mathbf{q}}|\Psi_0^A\rangle|^2 \\ &\quad = K 2\varepsilon_L [G_E^p(q_\mu^2)]^2 \hat{S}(\mathbf{p}_1',\mathbf{p}_2',E),\end{aligned} \tag{43}$$

i.e., it is proportional to the combination of spectral functions given in Eq. (42). In Eq. (43) the symbols K, ε_L, and G_E^p represent a kinematical factor, the longitudinal polarization, and the electric form factor of the proton, respectively [9]. This longitudinal cross section is plotted in Figs. 11 and 12 for the 0^+ ground state and the first excited 2^+ state of ^{12}C, respectively, and for the same kinematics as adopted in the calculations of Refs. [9,10]. In this coplanar setting the virtual photon momentum **q** is by definition along the z axis, while the two detected protons are in the x-z plane at equal angles with respect to **q**. By varying this angle γ_{pq}, one is able to vary the relative and center-of-mass momenta of the pair simultaneously.

Our results agree with those for the OMY and KK potentials in Fig. 1 of Ref. [10] for angles larger than 50°. For smaller angles the cross section is largely spurious, due to the use of plane waves for the knocked-out protons in the final states, instead of waves orthogonalized to the bound states. This spuriosity of the cross section is clearly indicated by the fact that for the small angles the calculated curves are all roughly equal to the one labeled ''no SRC,'' calculated without defect functions. If there were neither short- nor long-range correlations, the cross section should be zero. Our separate treatment of short- and long-range correlations makes it difficult to give a reliable prediction for the angles below 50°, i.e., for initial proton momenta of about 1.5 fm^{-1}. These momenta are too large to be sufficiently covered by the limited shell model space in which we treat the long-range correlations, while they are too small to avoid the aforementioned problems with the Pauli operator in the Bethe-Goldstone equation. To stipulate this problem and because a more satisfactory treatment is outside the scope of this work, we present the results as displayed in Figs. 11 and 12 and shall further focus on the larger angles, corresponding to higher initial momenta, approximately 2 fm^{-1}, of the protons. For these momenta the predictions are more reliable.

The main features of Figs. 11 and 12 may be qualitatively understood from the range of center-of-mass momenta and relative momenta involved. The center-of-mass momentum becomes zero for $\gamma_{pq} \approx 56°$ and increases to 1.4 fm^{-1} at $\gamma_{pq} = 80°$. This explains why all curves have a dip around 56° in Fig. 12. In the dominant 2^+ configurations, the only

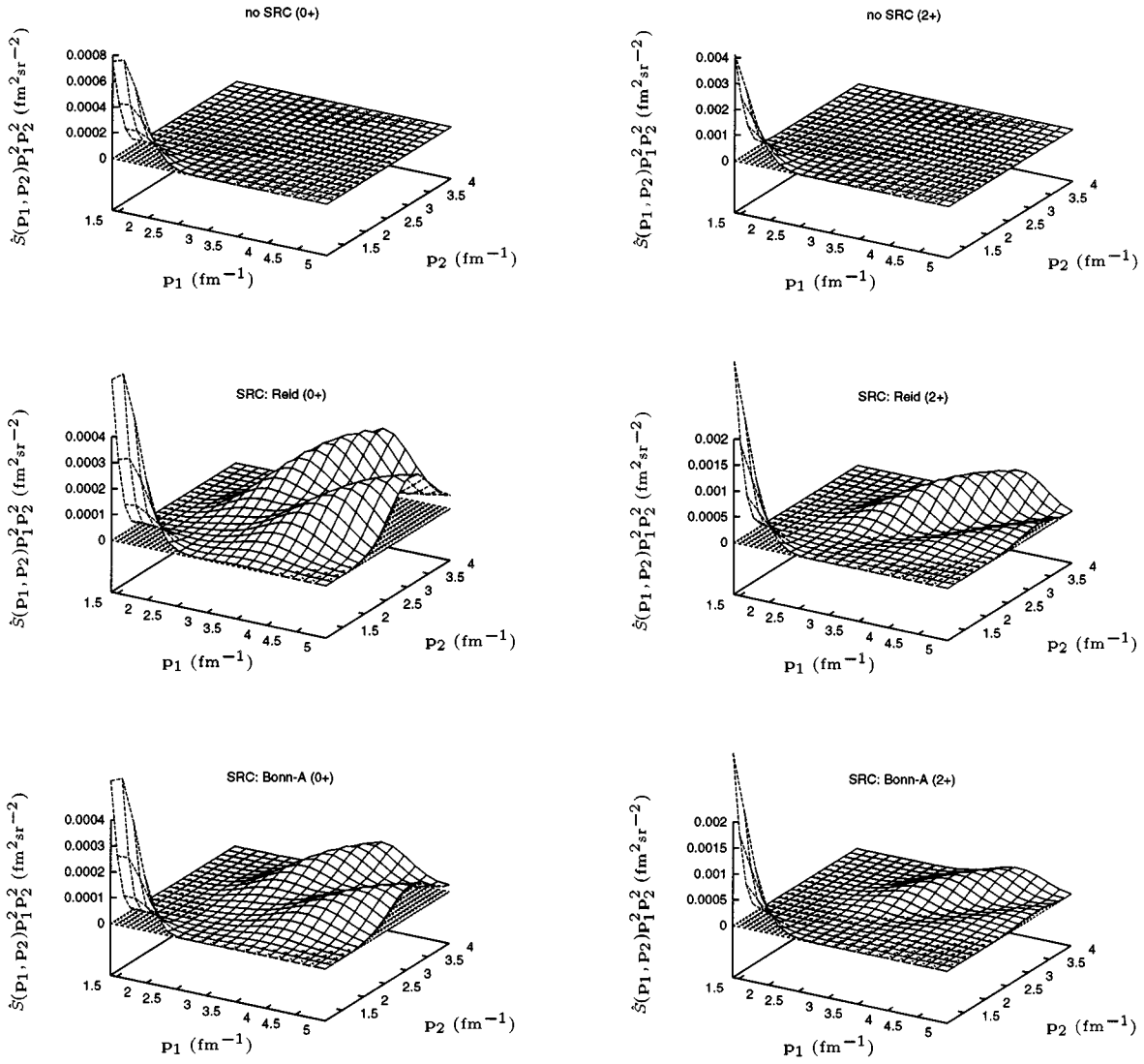

FIG. 9. Superposition of spectral functions (42) appropriate for the removal of two protons with final momenta $\mathbf{p}_1$ and $\mathbf{p}_2$ from ^{16}O leading to the final 0^+ ground state or first excited 2^+ state in ^{14}C. The plots are given for a kinematic setting used in experiments at NIKHEF [14]. The momentum vector $\mathbf{q}$ is fixed along the z axis, with length 313 MeV/c. The momenta $\mathbf{p}_1$ and $\mathbf{p}_2$ are in the same plane with $\mathbf{q}$ at $-49°$ and 123° angles with respect to this transferred momentum, respectively. The upper plots correspond to harmonic oscillator wave functions without the inclusion of short-range correlations. In the lower plots these SRC's are incorporated by the defect functions of the Reid potential and the Bonn-A potential (see Fig. 1).

part with $L_{\text{c.m.}}=0$, and which is therefore nonzero for $p_{\text{c.m.}}=0$, is multiplied with a relative $^1D_2$ wave, which has negligible short-range correlations. The steep rise of the curves above 60° in Fig. 12 illustrates the importance of the $L_{\text{c.m.}}=2$ part in the 2^+ wave function, multiplied by the relative $^1S_0$ wave function. The difference between the Bonn, Reid, and Argonne potentials for $\gamma_{pq}=70°-80°$ in Fig. 12 may be traced back to the $^1S_0$ defect functions in Fig. 5. With the adopted value of 1.8 fm^{-1} for the proton momenta, the relative momentum $|\mathbf{p}_1 - \mathbf{p}_2|/2$ ranges from 1.8 fm^{-1} for $\gamma_{pq}=56°$ to 2.04 fm^{-1} for $\gamma_{pq}=80°$. Within this narrow range of momenta the $^1S_0$ defect function goes through zero for the Bonn potential while it is largest for the Argonne potential.

The trends shown in Fig. 11 for the 0^+ ground state may be understood by similar considerations. Those for OMY and KK potentials are the most obvious. These include only $^1S_0$ correlation functions. In the 0^+ configurations these go together with $L_{\text{c.m.}}=0$, which explains their maximum near $\gamma_{pq}=56°$, for which $p_{\text{c.m.}}=0$, and the rapid falloff with increasing $p_{\text{c.m.}}$ at larger angles. For the more realistic Bonn, Reid, and Argonne potentials the trend is different. This is due to the fact that the dominant $(1p\frac{1}{2})^{-2}$ component in the ground state is made up for two thirds of a $^3P_1$, $L_{\text{c.m.}}=1$ state. The $^3P_1$ defect function, shown in Fig. 5, is rather large around 2 fm^{-1} for the Bonn and Reid potentials and gives the main contribution for $\gamma_{pq}\approx 60°-70°$ in Fig. 11. This explains why the Argonne result is lower here, in spite of its larger $^1S_0$ defect function.

From these considerations it is clear that the ratios of predicted cross sections for different potentials depend on the probed momentum range. For larger relative momenta, $|\mathbf{p}_1-\mathbf{p}_2|/2\approx 3$ fm^{-1} or higher, one tests mainly the $^1S_0$ defect functions (squared), which give a factor of 2 larger cross

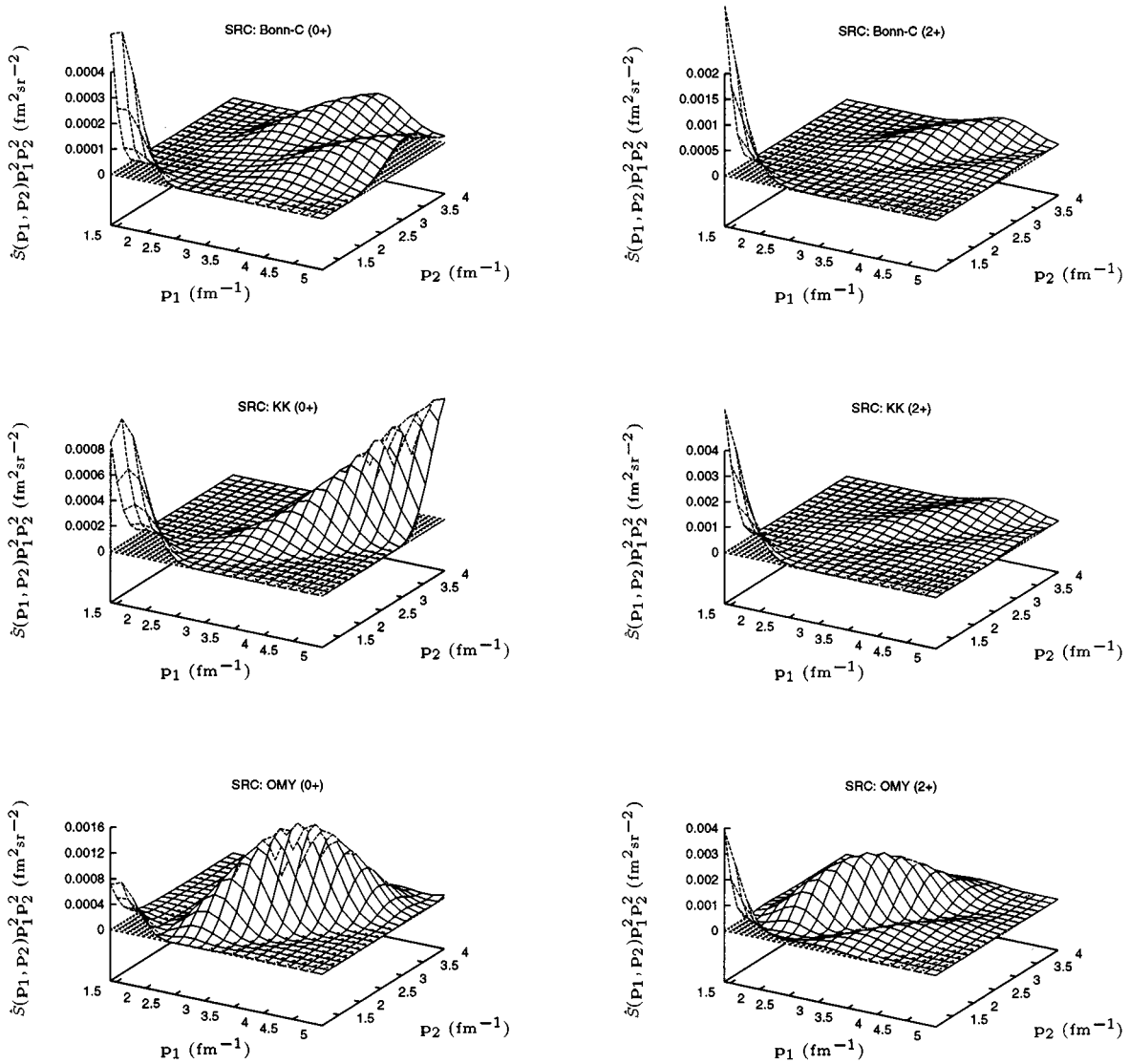

FIG. 10. Same as Fig. 9 but with short-range correlations from the defect functions of the Bonn-C potential (top) and the variational correlation functions (Fig. 3) from the KK (middle) or OMY interaction (bottom). Note that the vertical scale in the lower figures differs by a factor of 2 or 4 from the upper ones as well as from Fig. 9.

sections for the Reid than for the Bonn and Argonne potentials. This is outside the reach of the facilities at NIKHEF or Mainz, but might be possible at CEBAF. Before making strong recommendations in this direction, one should also consider contibutions from transverse and two-body currents. A careful study of these processes as well as the inclusion of distortion effects should be the subject of future investigations.

VI. CONCLUSIONS

The two-nucleon-removal spectral function of ^{16}O is studied with emphasis on the presence of high-momentum components in the relative wave function of the removed pair. These high momenta are introduced into shell model (relative) wave functions by the addition of defect functions calculated with the Bethe Goldstone equation [38] and by using correlation functions obtained from variational calculations [54]. Within the shell model space, consisting of four major shells, long-range correlations are treated with the dressed RPA (DRPA) method. The DRPA calculation of the two-nucleon-removal amplitudes, leading to the final states in ^{14}C, employs the G-matrix effective interaction from the Bonn-C potential. These amplitudes are used together with the defect or correlations functions to investigate the effect of short-range correlations on the two-nucleon-removal spectral function. It is found that at high momenta ($2-5$ fm^{-1}) the spectral function is roughly a factor of 2 larger when calculated with the defect functions of the Reid-soft-core potential than with those of the Bonn-A or Bonn-C potential (see Figs. 9 and 10). Distinct shapes and much larger differences for the spectral functions are obtained with the correlation functions, deduced from the older semirealistic KK and OMY NN potentials.

Since the ground state of ^{14}C is well separated from the

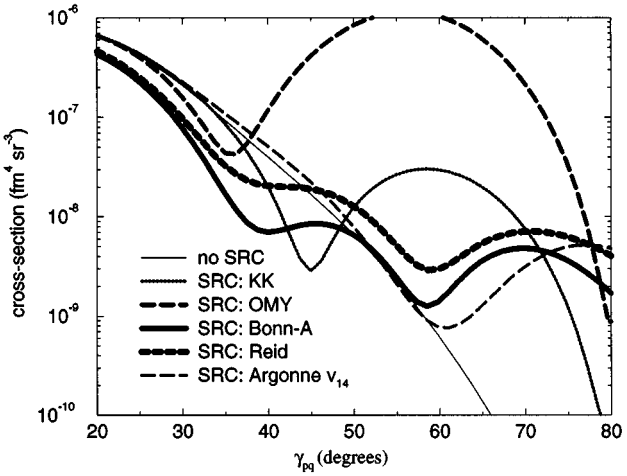

FIG. 11. Longitudinal ^{16}O$(e,e'pp)$ cross section in plane wave approximation (43) for the transition to the ground state of ^{14}C. The kinematical setup corresponds to a virtual photon momentum $\mathbf{q}$ which is directed along the z axis and has a magnitude of 2 fm^{-1}, and both proton momenta with magnitude 1.8 fm^{-1} detected at an angle γ_{pq}. The beam energy p_0 is 700 MeV, the transferred energy ω is 150 MeV, and the scattering angle of the electron is 34.8° with a corresponding virtual photon polarization of $\varepsilon = 0.81$. As explained in the text, the cross sections below 50° are largely spurious.

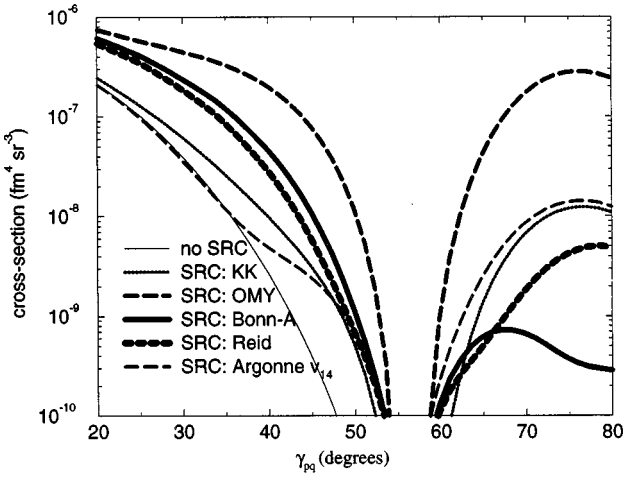

FIG. 12. Same cross section as in Fig. 11, but now for the transition to the first 2^+ state in ^{14}C.

excited states, a missing-energy resolution of 4 MeV in $(e,e'pp)$ experiments is sufficient to study its spectral function separately. The largest cross sections must be expected for the 2^+ states at about 7–8 MeV, however. This is indicated by the $^1S_0$ pair removal spectral function of Fig. 7. In the region of final states with negative parity, above 40 MeV, the ^3P contribution might be studied by filtering out the $L_{\text{c.m.}} = 0$ part (cf., Fig. 8) of the cross section. Although the ^3P defect functions are in general smaller than the $^1S_0$ defect function, they may yield the dominant contribution for the ^{14}C ground state under special kinematical conditions, as illustrated in Fig. 11 for angles $\gamma_{pq} \approx 75°–80°$. This may be traced back to a node in the $^1S_0$ defect functions for Bonn and Reid potentials at relative momentum $|\mathbf{p}_1 - \mathbf{p}_2|/2$ slightly below 2 fm^{-1}, shown in Fig. 5. For higher relative momenta, where the $^1S_0$ defect function is the dominant factor, the longitudinal cross section predicted with the Reid potential is roughly a factor 2 larger than for the Bonn and Argonne potentials. To probe this region one needs an electron beam of several GeV.

Before making strong recommendations for such experiments, one should also take other mechanisms into account than the spectator approximation [9] adopted here, though under suitable conditions they may turn out to be less important. Meson-exchange currents are suppressed for two-proton knockout as the exchanged meson is uncharged [10]. Experiments should be performed at low missing energies for the $A-2$ system in order to avoid the domination of the cross section by the excitation of the Δ resonance. For this reason it is also important to perform a separation of longitudinal and transverse cross sections. The contribution of charge exchange in the final state after the knockout of a proton-neutron pair may be suppressed in suitable kinematic conditions [12]. Final state interactions, notably absorption of the outgoing protons, have been neglected in Figs. 11 and 12. According to Ref. [12] this effect can be roughly represented by an overall reduction of the cross section by a factor of 2–3. Inclusion of these distortions and of other mechanisms will be explored in future work.

ACKNOWLEDGMENTS

We wish to thank Steve Pieper for supplying us with the Argonne v_{14} correlation functions. This work is part of the research program of the Foundation of Fundamental Research of Matter (FOM), which is financially supported by the Netherlands' Organization for Scientific Research (NWO). Additional support is provided by the U.S. National Science Foundation under Grant No. PHY-9307484 (at Washington University) and the ''Deutsche Forschungsgemeinschaft'' under Grant No. SFB 382.

[1] I. Bobeldijk *et al.*, Phys. Rev. Lett. **73**, 2684 (1994).
[2] K. I. Blomqvist *et al.*, Phys. Lett. B **344**, 85 (1995).
[3] H. Müther and W. H. Dickhoff, Phys. Rev. C **49**, R17 (1994).
[4] H. Müther, A. Polls, and W. H. Dickhoff, Phys. Rev. C **51**, 3051 (1995).
[5] K. Gottfried, Nucl. Phys. **5**, 557 (1958).
[6] C. Ciofi degli Atti, in *Two Nucleon Emission Reactions*, edited by O. Benhar and A. Fabrocini (ETS Editrice, Pisa, 1990), p. 1.
[7] O. Benhar, A. Fabrocini, and S. Fantoni, in *Two Nucleon Emission Reactions*, edited by O. Benhar and A. Fabrocini (ETS Editrice, Pisa, 1990), p. 49.
[8] S. Boffi, in *Two Nucleon Emission Reactions*, edited by O. Benhar and A. Fabrocini (ETS Editrice, Pisa, 1990), p. 87.

[9] C. Giusti and F. D. Pacati, Nucl. Phys. **A535**, 573 (1991).
[10] C. Giusti, F. D. Pacati, and M. Radici, Nucl. Phys. **A546**, 607 (1992).
[11] C. Giusti and F. D. Pacati, Nucl. Phys. **A571**, 694 (1994).
[12] C. Giusti and F. D. Pacati, Nucl. Phys. **A585**, 618 (1995).
[13] L. J. H. M. Kester *et al.*, Phys. Rev. Lett. **74**, 1712 (1995).
[14] Spokespersons W. H. A. Hesselink and E. Jans, NIKHEF-K Proposal NR:94-1 (unpublished).
[15] J. Ryckebusch, Nucl. Phys. **A568**, 828 (1994).
[16] A. R. Edmonds, *Angular Momentum in Quantum Mechanics* (Princeton University Press, Princeton, 1957).
[17] P. J. Brussaard and P. W. M. Glaudemans, *Shell-Model Applications in Nuclear Spectroscopy* (North-Holland, Amsterdam, 1977).
[18] A. L. Fetter and J. D. Walecka, *Quantum Theory of Many Particle Physics* (McGraw-Hill, New York, 1971).
[19] J. W. A. den Herder, H. P. Blok, E. Jans, P. H. M. Keizer, L. Lapikás, E. N. M. Quint, G. van der Steenhoven, and P. K. A. de Witt Huberts, Nucl. Phys. **A490**, 507 (1988).
[20] E. N. M. Quint, Ph.D. thesis, NIKHEF, Amsterdam, 1988.
[21] G. J. Kramer, Ph.D. thesis, NIKHEF, Amsterdam, 1990.
[22] G. van der Steenhoven, Nucl. Phys. **A527**, 17c (1991).
[23] L. Lapikás, Nucl. Phys. **A553**, 297c (1993).
[24] M. Leuschner *et al.*, Phys. Rev. C **49**, 955 (1994).
[25] A. A. Abrikosov, L. P. Gorkov, and I. E. Dzyaloshinski, *Methods of Quantum Field Theory in Statistical Physics* (Dover, New York, 1975).
[26] M. G. E. Brand, G. A. Rijsdijk, F. A. Muller, K. Allaart, and W. H. Dickhoff, Nucl. Phys. **A531**, 253 (1991).
[27] G. A. Rijsdijk, K. Allaart, and W. H. Dickhoff, Nucl. Phys. **A550**, 159 (1992).
[28] G. A. Rijsdijk, W. J. W. Geurts, M. G. E. Brand, K. Allaart, and W. H. Dickhoff, Phys. Rev. C **48**, 1752 (1993).
[29] D. van Neck, M. Waroquier, and J. Ryckebusch, Nucl. Phys. **A530**, 347 (1991).
[30] W. J. W. Geurts, K. Allaart, W. H. Dickhoff, and H. Müther, Phys. Rev. C **53**, 2207 (1996).
[31] A. Ramos, A. Polls, and W. H. Dickhoff, Nucl. Phys. **A503**, 1 (1989).
[32] O. Benhar, A. Fabrocini, and S. Fantoni, Nucl. Phys. **A505**, 267 (1989).
[33] B. E. Vonderfecht, W. H. Dickhoff, A. Ramos, and A. Polls, Phys. Rev. C **44**, R1265 (1991).
[34] H. S. Köhler, Nucl. Phys. **A537**, 64 (1992).
[35] M. Baldo, I. Bombaci, G. Giansiracusa, U. Lombardo, C. Mahaux, and R. Sartor, Nucl. Phys. **A545**, 741 (1992).
[36] O. Benhar, A. Fabrocini, and S. Fantoni, Nucl. Phys. **A550**, 201 (1992).
[37] B. E. Vonderfecht, W. H. Dickhoff, A. Ramos, and A. Polls, Nucl. Phys. **A555**, 1 (1993).
[38] H. Müther and P. U. Sauer, in *Computational Nuclear Physics*, edited by K.-H. Langanke, J.A. Maruhn, and S.E. Koonin, (Springer, New York, 1993).
[39] K. A. Brueckner, J. L. Gammel, and H. Weitzner, Phys. Rev. **110**, 431 (1958).
[40] K. A. Brueckner, A. M. Lockett, and A. M. Rotenberg, Phys. Rev. **121**, 255 (1961).
[41] A. de-Shalit and I. Talmi, *Nuclear Shell Theory* (Academic, New York, 1963).
[42] T. A. Brody and M. Moshinsky, *Tables of Transformation Brackets: For nuclear shell-model calculations* (Universidad Nacional Autonoma de Mexico, Mexico D.F., 1960).
[43] M. Sotona and M. Gmitro, Comput. Phys. Commun. **3**, 53 (1972).
[44] R. Machleidt, Adv. Nucl. Phys. **19**, 1 (1989).
[45] R. V. Reid, Ann. Phys. (N.Y.) **50**, 411 (1968).
[46] J. W. Clark and E. Feenberg, Phys. Rev. **113**, 388 (1959).
[47] R. Jastrow, Phys. Rev. **98**, 1479 (1955).
[48] J. W. Clark, Prog. Part. Nucl. Phys. **2**, 89 (1979).
[49] V. R. Pandharipande and R. B. Wiringa, Rev. Mod. Phys. **51**, 821 (1979).
[50] J. W. Clark, in *The Many-Body Problem: Jastrow correlations versus Brueckner theory*, edited by R. Guardiola and J. Ros (Springer, New York, 1981), p. 184.
[51] A. Kallio and K. Kolltveit, Nucl. Phys. **53**, 87 (1964).
[52] T. Ohmura, N. Morita, and M. Yamada, Prog. Theor. Phys. **15**, 222 (1956).
[53] S. Fantoni and V. R. Pandharipande, Phys. Rev. C **37**, 1988 (1988).
[54] S. C. Pieper, R. B. Wiringa, and V. R. Pandharipande, Phys. Rev. C **46**, 1741 (1992).
[55] C. C. Gearhart, Ph.D. thesis, Washington University, St. Louis, 1994.
[56] C. C. Gearhart, W. H. Dickhoff, A. Polls, and A. Ramos (unpublished).
[57] R. B. Wiringa, R. A. Smith, and T. L. Ainsworth, Phys. Rev. C **29**, 1207 (1984).
[58] W. J. W. Geurts, Ph.D. thesis, Vrije universiteit, Amsterdam, 1996.
[59] K. Allaart, P. J. Ellis, W. J. W. Geurts, Jifa Hao, T. T. S. Kuo, and G. A. Rijsdijk, Phys. Rev. C **47**, 895 (1993).
[60] F. Ajzenberg-Selove, Nucl. Phys. **A523**, 1 (1991).
[61] F. Ajzenberg-Selove, Nucl. Phys. **A460**, 1 (1986).
[62] D. G. Fleming, J. C. Hardy, and J. Cerny, Nucl. Phys. **A162**, 225 (1971).
[63] J. A. Macdonald, J. Cerny, J. C. Hardy, H. L. Harney, A. D. Bacher, and G. R. Plattner, Phys. Rev. C **9**, 1694 (1974).
[64] L. J. H. M. Kester, Ph.D. thesis, NIKHEF, Amsterdam, 1993.
[65] G. A. Rijsdijk, W. J. W. Geurts, K. Allaart, and W. H. Dickhoff, Phys. Rev. C **53**, 201 (1996).